AIAA JOURNAL
Vol. 34, No. 12, December 1996

Turbulence Measurements in a Mach 2.9 Boundary Layer Including Mild Pressure Gradients

Rodney D. W. Bowersox* and Thomas A. Buter†
U.S. Air Force Institute of Technology, Wright–Patterson Air Force Base, Ohio 45433-7765

Mass-weighted-time, or Favre-averaged, turbulence measurements were acquired in a Mach 2.9 air boundary layer for three pressure gradient cases. Curved walls were used to produce the pressure gradient and streamline curvature effects. The boundary layers along a curved wall expansion ($\beta \approx -0.5$ and $Re_\theta = 14.5 \times 10^3$), the expansion region ($\beta \approx -1.2$ and $Re_\theta = 11.5 \times 10^3$) following an initial compression ($\beta \approx 1.0$), and a nominally zero pressure gradient ($Re_\theta = 10.9 \times 10^3$) were investigated. Laser Doppler velocimetry and cross-film anemometry were used to acquire direct and detailed surveys of the Reynolds shear stress ($\overline{\rho u'v'}$) and the mean transverse Favre velocity fluctuation ($\overline{v''}$). Velocity profiles were also acquired. The magnitude and distribution of the turbulent shear stress was found to be strongly affected by the pressure gradients. When compared with the zero pressure gradient results, the favorable pressure gradient was observed to significantly reduce the shear stress magnitude (50–100% across the boundary layer), which was consistent with the reported stabilizing effect of the expansion wave on the turbulent flow structure. The effects of the "combined" pressure gradient on the shear stress profile was not as pronounced (nominal 20% increase). In both cases, the overall magnitude of the $\overline{v''}$ component was dramatically increased: a nominal increase of 170% for the favorable pressure gradient and 300% for the combined flow.

Nomenclature

h	= tunnel height
M	= Mach number
P	= production
P_w	= pressure work
p	= pressure
Re	= Reynolds number
T	= temperature
U	= mean Farve-averaged axial velocity
u, v, w	= velocity components
u^*	= friction velocity $[\sqrt{(\tau_w/\rho_w)}]$
x, y, z	= Cartesian coordinates
y^+	= $\rho_w u^* y/\mu_w$
β	= $\delta^*/\tau_w \, dp/dx$
δ	= boundary-layer thickness
δ^*	= kinematic displacement thickness
θ	= kinematic momentum thickness
ρ	= density
τ	= shear stress

Subscripts

e	= boundary-layer edge
t	= total condition
w	= wall
∞	= freestream condition

Superscripts

F	= Favre
i	= incompressible component
R	= Reynolds
$''$	= Favre fluctuating component
$'$	= Reynolds fluctuating component
$\bar{}$	= Reynolds mean component

Received May 5, 1995; revision received April 10, 1996; accepted for publication Aug. 22, 1996; also published in *AIAA Journal on Disc*, Volume 2, Number 1. This paper is declared a work of the U.S. Government and is not subject to copyright protection in the United States.

*Assistant Professor, Department of Aeronautics and Astronautics, Graduate School of Engineering. Member AIAA.

†Assistant Professor, Department of Aeronautics and Astronautics, Graduate School of Engineering. Senior Member AIAA.

Introduction

SUPERSONIC turbulent wall boundary layers subjected to a pressure gradient arise in many situations of practical interest. For example, the exterior curved surfaces of high-speed flight vehicles or missiles, supersonic aircraft engine inlets, and the flow within high-performance compressors or turbofans may experience a supersonic, pressure gradient, turbulent boundary layer. Such flows are typically intractable from an analytical standpoint and challenging from either an experimental or numerical perspective.

At the present time, simulation of such flows are limited by the accuracy of turbulence modeling methodology. Given the lack of computational resources necessary to directly solve and/or perform a large eddy simulation of high Reynolds number turbulent flows, engineers must rely on an approximate averaged form of the governing Navier–Stokes equations. The prevailing approximating techniques are the Reynolds time and Favre mass-weighted time averaging.[1] Of the two, Favre averaging is almost universally adopted for compressible flows. The benefit of Favre averaging over the standard Reynolds averaging is that the explicit appearance of the density–velocity correlations in the Navier–Stokes equations is eliminated. The second-order components of the Favre- and Reynolds-averaged turbulent shear stresses are given by

$$\tau_{ij}^F = -\bar{\rho}\overline{u_i'' u_j''}, \qquad \tau_{ij}^R = -\bar{\rho}\overline{u_i' u_j'} - \bar{u}_i\overline{\rho' u_j'} - \bar{u}_j\overline{\rho' u_i'} \quad (1)$$

As can be inferred from Eq. (1), the compressible Favre-averaged Navier–Stokes equations are similar in appearance to the incompressible Reynolds-averaged form. This fact coupled with Morkovin's hypothesis,[2] which states that "... the essential dynamics supersonic boundary layers follow the incompressible pattern," has led researchers to extend incompressible turbulence models to compressible flows on a largely ad hoc basis. As reported in Spina et al.,[3] Morkovin's hypothesis is taken to be valid if the fluctuating Mach number M' is small (i.e., $M'/\bar{M} < 0.3$). It has generally been accepted practice to neglect compressibility effects for $M < 5.0$ (Ref. 4). The effort to develop "compressibility effect" corrections to incompressible models has been extensive.[5–8] However, Spina et al.[3] report that the dynamics of the turbulent boundary layer may be affected by compressibility at lower Mach numbers than previously believed. Further, Smits et al.[9] compared the structure of an incompressible and a supersonic ($M = 2.9$) boundary layer. Their measurements indicated "... that despite broad similarities, the turbulence structure of supersonic and subsonic boundary layers display significant differences."[9] Some of the differences may be

explained via an examination of the equation governing the transport of the Favre-averaged turbulent shear stress [Eq. (1)].

The familiar form of the Favre-averaged turbulent shear stress equation is given by[10]

$$\frac{\partial \tau_{ij}^F}{\partial t} + \frac{\partial}{\partial x_k}\left(U_k \tau_{ij}^F\right) = -P_{ij} + \varepsilon_{ij} + \Pi_{ij} + \frac{\partial}{\partial x_k}[-(\overline{\tau_{kj}u_i'' + \tau_{ki}u_j''}) + C_{ijk}] + \overline{u_i''}\frac{\partial \bar{p}}{\partial x_j} + \overline{u_j''}\frac{\partial \bar{p}}{\partial x_i} \qquad (2)$$

where τ_{ij} is the laminar viscous shear stress tensor, P_{ij} is the usual production term, Π_{ij} is the pressure-strain redistribution term, ε_{ij} is the dissipation, and C_{ijk} is termed the turbulent transport term.[10] The last two terms in Eq. (2) are commonly referred to as the pressure work terms and arise because, for compressible flows, $\overline{u_i''} \neq 0$. Since the presence of these terms is a direct result of compressibility, researchers do not have the luxury of an incompressible database upon which to build models. Measurements of any of the terms in Eq. (2) are rare. Thus, to develop models for these terms, researchers have primarily relied on intuition or some approximate analytical method. For example, the strong Reynolds analogy and applied rapid distortion theory[11,12] have been used to obtain reasonably accurate predictions for the effects of bulk dilatation on the Reynolds shear stress. Nonetheless, modeling efforts of this sort suffer from a lack of experimental data.

Though the structure of the subsonic and supersonic boundary layers with and without pressure gradient has been extensively studied,[2-4,11-21] experimental investigations that provide Favre-averaged turbulence quantities are rare. Thus, the objective of the present research was to directly measure the mean transverse Favre fluctuation velocity ($\overline{v''}$) and the Favre turbulent shear stresses ($\bar{\rho}\overline{u''v''}$). Laser Doppler velocimetry and cross-film anemometry were utilized to obtain these data. A Mach 2.9 turbulent boundary-layer flow was studied. Curved walls were used to generate mild pressure gradients: an expansion ($\beta \approx -0.5$) and an expansion ($\beta \approx -1.2$) following a compression ($\beta \approx 1.0$). Measurements were obtained across the boundary layers for each of the two aforementioned curved walls. In addition, the zero pressure gradient tunnel boundary layer was surveyed for comparative purposes.

Experimental Apparatus

Facilities

All tests were performed in the U.S. Air Force Institute of Technology supersonic wind tunnel. This blowdown, pressure-vacuum system provided 25-s test times at Mach 2.9, with a ±0.02 variation across the test section. The settling chamber pressure and temperature were maintained at 2.0 ± 0.03 atm and 294 ± 2 K for all tests. The freestream $Re/m = 15 \times 10^6$. The freestream turbulent kinetic energy was 0.016% of the mean specific kinetic energy. The test section was 6.35 × 6.35 cm in cross section. The coordinate system was defined such that x was positive in the streamwise direction, and the origin was located at the nozzle throat. Since all of the measurements were made normal to the tunnel ceiling, y was defined as positive down, and it was zero at the test section ceiling; z completed the right-hand system.

The curved wall sections were built into the tunnel ceiling, and the contours started at $x = 65.08$ cm. The curved wall contours were generated to match a cubic polynomial:

$$\Delta h(\text{cm}) = a_0 + a_1\Delta x + a_2\Delta x^2 + a_3\Delta x^3$$

where Δh was relative to the tunnel ceiling, and $\Delta x(\text{cm}) = x - 60.0$. The coefficients for the combined pressure gradient (CPG) and favorable pressure gradient (FPG) curved walls are given in Table 1. The tunnel height above the lower floor is shown in Fig. 1. The measurements normal to the curved wall were acquired at $x = 71.0$ and 71.5 cm for the CPG and FPG models, respectively. The zero pressure gradient data were also taken at $x = 71.5$ cm downstream of the nozzle throat. These measurement locations were nominally 3500 momentum thickness heights downstream of the nozzle exit, and hence it is expected that the boundary layer had reached a state of equilibrium.

Table 1 Model contours

Model	$a_0 \times 1$	$a_1 \times 10$	$a_2 \times 100$	$a_3 \times 1000$
FPG	−0.2078	0.8970	−0.9476	−0.03598
CPG	1.186	−5.410	7.478	−2.800

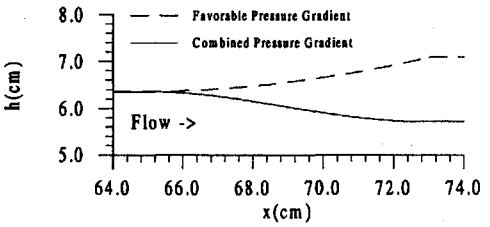

Fig. 1 Schematic of pressure gradient curved wall contours.

Instrumentation

A Dantec brand 57N enhanced Burst Spectrum Analyzer two-component laser Doppler velocimetry system, with a 300-mW argon-ion laser, was used for the present experiment. The $1/e^2$ beam diameter was 0.82 mm. The green beams (514.5 nm) and blue beams (418.0 nm) were aligned parallel and perpendicular to the model walls, respectively. This was done to avoid the angular bias reported in Ref. 18. A 40-MHz frequency shift was applied across both the green and blue components. A 600-mm focal-length transmitting lens was used; this provided a 0.276-mm diam control volume that was 0.9 cm long (along the z axis). Because of the increased intensity of the scattered light, forward scattering was used. However, to prevent damaging the photomultiplyer tubes, the system was operated at 3.5 deg off axis. The Dantec three-dimensional traverse system was used. The rated accuracy was ±80 μm.

The flow was seeded by injecting 0.6-μm particles of olive oil along the centerline of the tunnel upstream of the flow straightners within the stilling chamber. The particles were generated with a TSI brand six jet atomizer. Random error uncertainty analysis indicated a ±9.0 and 8.0% scatter in the mean velocity and Reynolds shear stress measurements, respectively. The largest source of uncertainty was related to a 0.01-mm scatter in the traverse position.

TSI brand Intelligent Flow Analyzer 100 constant temperature anemometer systems were used with cross-film sensors. The TSI 1243-20 platinum hot-film sensors each had a length of 1.0 mm and a diameter of 51 μm. The cross-film probe area was nominally 1.0 mm^2. The frequency response was optimized to nominally 120 kHz by the square wave technique in the Mach 2.9 freestream. The data presented here were taken using the single overheat technique.[22] However, multiple overheat data were also acquired, and comparison with the single overheat results indicated that the results agreed to within the expected experimental scatter.[13]

Data Reduction

The cross-film data reduction techniques were founded in the analyses of Kovasznay[23] and Spangenberg.[24] In general, the reduction was based on the empirical heat loss formula (King's law)

$$Nu = a\sqrt{Re_e} + b$$

where Re_e is the effective cooling Reynolds number.[22] As in Bowersox and Schetz,[25] the cosine law was assumed valid since the flow angles in the present thin layer type flow were not expected to deviate substantially from those of the calibration. The sensors were calibrated by placing them in the freestream and varying the tunnel total pressure. Other researchers have developed modified forms of the preceding heat transfer law for supersonic flow.[26] However, since the minimum linear regression correlation coefficient for all of the present cross-film calibrations was 0.993, King's law was deemed appropriate.

Cross-film anemometry provided a direct measurement of

$$\overline{(\rho u)'(\rho v)'}$$

The compressible Reynolds turbulent shear stresses [Eq. (1)] were related to the mass flux fluctuation correlation by the following identity[25]:

$$\frac{\tau_{xy}^{R}}{\bar{\rho}\tilde{u}^2} \equiv -\frac{\overline{(\rho u)'(\rho v)'}}{(\overline{\rho u})^2} + \bar{\rho}\tilde{u}\tilde{v}\overline{\left(\frac{\rho'}{\bar{\rho}}\right)^2} \tag{3}$$

where third-order correlations were neglected. For thin layer type flows, the second term on the right-hand side is usually much smaller than the first. This has been verified for the present flows,[13] where the second term was estimated to be nominally 1–5% of the first.

Laser Doppler velocimetry (LDV) provided direct measurements of the mean velocity and the kinematic Reynolds shear stress {i.e., first term on the right-hand side of the Reynolds shear stress [Eq.(1)]}:

$$\frac{\tau_{xy}^{i}}{\bar{\rho}\tilde{u}^2} = -\frac{\overline{u'v'}}{\tilde{u}^2} \tag{4}$$

The kinematic Reynolds shear stress is related to the Favre shear stress by the following identity:

$$\bar{\rho}\overline{u''v''} \equiv \bar{\rho}\overline{u'v'} + \bar{\rho}\overline{u''}\,\overline{v''} \tag{5}$$

where $\overline{u_i''} = -\overline{\rho' u_i'}/\bar{\rho}$. Thus for homogeneous gaseous flows where $\rho'/\bar{\rho}$ is expected to be on the order of $\frac{1}{10}$, the second term on the right-hand side of Eq. (5) is fourth order. Hence, it can be neglected with respect to the second-order shear stresses, which allowed a measurement of the Favre shear stress with the LDV technique.

Finally, for thin layer flows where $\bar{v}/\tilde{u} \ll 1.0$, the laser Doppler and cross-wire data can be combined to yield direct measurements of the mean transverse Favre velocity fluctuation. Hence Eqs. (1), (3), and (4) can be combined to give

$$-\frac{\overline{\rho'v'}}{\bar{\rho}\tilde{u}} = \frac{\overline{v''}}{U} = \frac{\overline{u'v'}}{\tilde{u}^2} - \frac{\overline{(\rho u)'(\rho v)'}}{(\overline{\rho u})^2} \tag{6}$$

Results and Discussion

Mean Flow Results

The measured flow conditions are summarized in Table 2. The zero pressure gradient freestream conditions ($x = 71.5$ cm) were used as the reference upon which the effects of the pressure gradient/streamline curvature could be assessed. As expected, the velocity boundary-layer momentum and displacement thickness heights were found to increase as a result of both the wall curvature streamline divergence and the effects of the favorable pressure gradient on the density field.[3] The boundary-layer thicknesses for the combined pressure gradient flow were found to be similar to the zero pressure gradient results. Figure 2 presents the measured wall pressures along each model. The pressure gradient along the wall at the measurement locations was estimated from these data, and they are also provided in Table 2.

Table 2 Flowfield parameters

Model	M_e	dp_w/dx, Pa/m	Re_θ	θ, mm	δ^*, mm	τ_w, Pa	β
ZPG	2.79	0.2×10^4	1.1×10^4	0.50	0.61	70.0	0.02
FPG	2.91	-2.6×10^4	1.5×10^4	0.56	0.89	44.0	−0.5
CPG	2.51	-1.8×10^5	1.2×10^4	0.45	0.57	85.0	−1.2

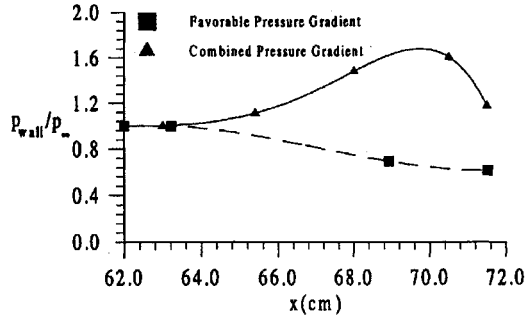

Fig. 2 Wall pressure contours (uncertainty: ±2%).

Since, as discussed later, LDV measurements were obtained in the logarithmic portion of the boundary layer, the wall shear stress was estimated by applying the Couette flow assumption in the near-wall region. Thus,

$$\tau_{xy}^{F} = \tau_w + \frac{dp_w}{dx}y$$

The wall shear stress values summarized in Table 2 were estimated with the preceding relation. In an attempt to validate the present results, the van Driest II skin-friction correlation[27] was used to estimate the wall shear stress. To perform the analysis, it was assumed that the zero pressure gradient flow could be modeled as a flat plate with its origin at $x = 0$. Based on this analysis, the wall shear was estimated as 67.0 Pa. The excellent agreement, 4.3%, was well within the expected ±10% uncertainty of the correlation.[27]

Estimates of the Clauser[20] pressure gradient parameter β are given in Table 2. Because of the natural growth of the tunnel boundary layers, there existed a very slight adverse pressure increase ($\beta = 0.02$). However, this was considered negligible, and these data were used as the zero pressure gradient comparison case. The favorable pressure gradient was also very mild ($\beta = -0.5$). Though the pressure gradients of the combined flow ($\beta = 1.0$ and -1.2) were much stronger than that of the favorable pressure gradient, β values of ±1.0 are also generally considered to be mild. As will be shown later, the effects of these mild pressure gradients on the turbulent flow structure were dramatic.

Presented in Fig. 3 are the axial velocity profiles for each of the three flow conditions. The minimum measured y^+ locations for each data set were estimated as 100, 50, and 200 for the zero, favorable, and combined pressure gradient boundary layers, respectively. As can be inferred from Fig. 3, for the present scaling the inner region of the boundary-layer velocity profile was most affected by the pressure gradient.

Turbulence Results

Shown in Fig. 4 is a comparison of the present zero pressure gradient turbulent shear stress measurements [filled circles—laser Doppler ($x = 71.5$ cm) and filled squares—cross-film ($x = 44$ cm)] to the Mach 2.9 boundary-layer results of Robinson et al.[17] and Elena and LeCharme[18] and the incompressible data of Klebanoff.[19] The overall qualitative agreement of the present results to the previous data is quite good. Because of the uncertainties associated with the wall shear stress, boundary-layer thickness, and turbulent shear stresses, the relatively large scatter in Fig. 4 is reasonable. The cross-film shear stress results were deduced from the cross-film output by assuming that the static pressure fluctuations were zero.[21] The agreement between the present data sets at two x locations indicated that the boundary layer had reached a state of equilibrium. With the measurement techniques validated, the effects of the pressure gradient/streamline curvature were investigated.

Compared in Fig. 5 are the incompressible Reynolds-averaged [or Favre-averaged, see Eq. (5)] turbulent shear stresses measured with the laser Doppler velocimeter. Compared with the zero pressure gradient results (filled circles), the favorable pressure gradient

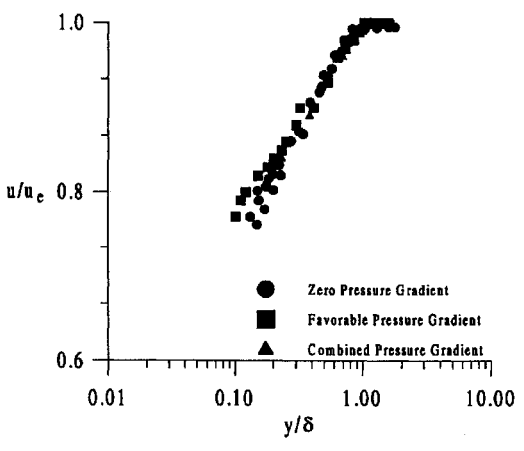

Fig. 3 Velocity profiles (uncertainty: ±9.0%).

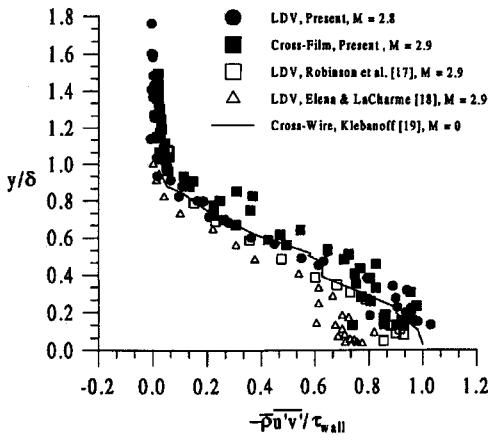

Fig. 4 Zero pressure gradient turbulent shear stresses.

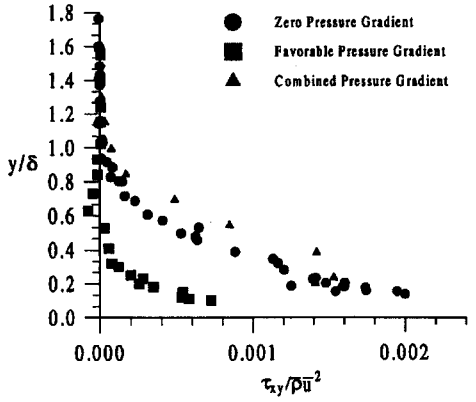

Fig. 5 Turbulent shear stress profiles (uncertainty: ±8.0).

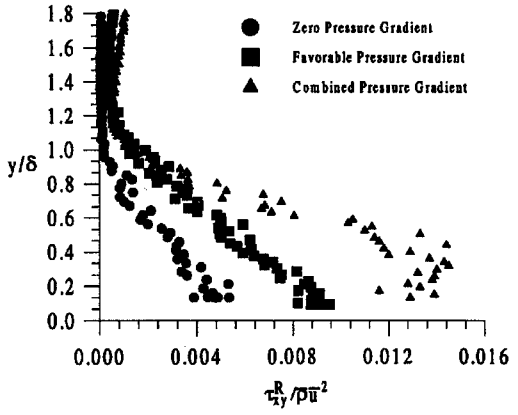

Fig. 6 Reynolds-averaged turbulent shear stress (uncertainty: ±13.0%).

boundary-layer shear stress magnitudes (filled squares) were reduced by 50–100%, depending on location within the boundary layer. In fact, over the top half of the boundary layer, the turbulent shear stresses were essentially zero. This decrease in the turbulent shear stress adds credence to the notion that a favorable pressure gradient tends to stabilize the flow.[3–12] The combined pressure gradient turbulent shear stresses (filled triangles) were found to be very similar in magnitude to the zero pressure gradient results. For this case, the flow first experiences a destabilizing compression, followed by the stabilizing expansion, and since the strength of each pressure gradient, based on the Clauser parameter, was nominally equal and opposite, the relatively small differences in the shear stresses were not overly surprising.

Presented in Fig. 6 are the Reynolds-averaged shear stresses measured with the cross-film [see Eq. (3)]. Comparing to the zero pressure gradient results, one can see that the overall Reynolds shear stress was increased for both nonzero pressure gradients. This is in

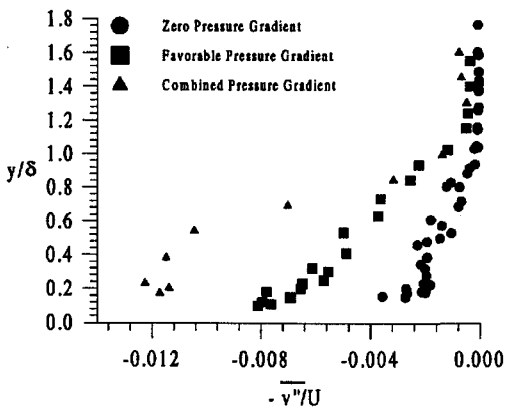

Fig. 7 Mean transverse Favre-averaged velocity fluctuation (uncertainty: ±21.0%).

direct contrast to the results in Fig. 5. The effects of the pressure gradients on the $\bar{u}\overline{\rho' v'}$ term on the right-hand side of the Reynolds shear stress [Eq. (1)] were deemed responsible for the measured increases. This notion is consistent with the results of Morkovin.[28] To better assess this phenomenon, this term was isolated as described by Eq. (6). The results are given in Fig. 7. Note the increase in $\overline{v''}$ of approximately 170 and 300% for the favorable and combined pressure gradient flows, respectively.

An equation governing the transport of the mean Favre velocity fluctuations is obtained by combining the fluctuating momentum and continuity equations,

$$\frac{\partial(\bar{\rho}\overline{u_i''})}{\partial t} + \frac{\partial(\bar{\rho}U_k\overline{u_i''})}{\partial x_k} = -\bar{\rho}\overline{u_k''}\frac{\partial \bar{u}_i}{\partial x_k} - \frac{\partial \tau^F_{ik}}{\partial x_k} - \bar{\rho}\overline{u_k''}\frac{\partial u_i''}{\partial x_k} + \frac{\partial(\overline{\rho' u_i'' u_k''})}{\partial x_k} - \overline{\frac{\rho'}{\bar{\rho}}\left(\frac{\partial \tau'_{ik}}{\partial x_k} - \frac{\partial p'}{\partial x_i}\right)} + \overline{\left(\frac{\rho'}{\bar{\rho}}\right)^2}\left(\frac{\partial \bar{\tau}_{ik}}{\partial x_k} - \frac{\partial \bar{p}}{\partial x_i}\right) \tag{7}$$

Note that the arguments previously used to relate the Favre and incompressible component of the Reynolds shear stress were again applied. The first and last terms on the right-hand side of Eq. (7) can be taken to represent the mean flow production. For the transverse component, with the molecular shear stress neglected, these terms reduce to

$$P'' = -\bar{\rho}\left(\overline{u''}\frac{\partial V}{\partial x} + \overline{v''}\frac{\partial V}{\partial y}\right) - \overline{\left(\frac{\rho'}{\bar{\rho}}\right)^2}\frac{\partial \bar{p}}{\partial y}$$

where P'' was defined to represent the production of $\overline{v''}$. The pressure gradient across the boundary layer due to the streamline curvature can be estimated by

$$\frac{\partial p}{\partial y} = -\frac{\rho u^2}{R}$$

where R is the radius of curvature of the flow turning. For the favorable pressure gradient model, $\delta \approx 1.28$ cm and $R = 48$ cm. Hence using the boundary-layer edge conditions to obtain a representative value, then $\partial p/\partial y \approx -160.0$ kPa/m. For the present mild favorable pressure gradient flows, the strain rates in the first term on the right-hand side of P'' can reasonably be assumed to be much smaller that the pressure gradient term. Thus, the production due to the streamline curvature was an important factor affecting $\overline{v''}$. For the combined pressure gradient model, $\delta \approx 0.75$ cm and $R = 29$ cm, leading to $\partial p/\partial y \approx -360.0$ kPa/m.

Referring back to Eq. (2), one can assess the relative importance of the production and pressure work terms in the turbulent shear stress transport. The largest production term [$\mathcal{O}(\delta)$] for the x–y component of the shear stress for boundary-layer type flows is given by

$$P = \tau^F_{yy}\frac{\partial \bar{u}}{\partial y} \approx -2\tau^F_{yx}\frac{\partial \bar{u}}{\partial x}$$

where the second approximation was based on empirical evidence.[29] In addition, the pressure work term reduces to

$$P_w = \overline{u''}\frac{\partial p}{\partial y} + \overline{v''}\frac{\partial p}{\partial x}$$

where for mild pressure gradients the first term can be expected to be much larger than the second. Assuming that the strong Reynolds analogy holds for the present adiabatic flows and that $u'' \sim v''$, then the ratio of the pressure work to the production can be estimated as

$$P_w/P \approx -[(\gamma - 1)/2]M_e^2(\delta/R)$$

Hence, $P_w/P \approx 5.0$ and 16.0% for the favorable and combined pressure gradient flows, respectively.

The dramatic changes in the turbulent shear stresses have often been attributed to the additional strain rate terms in the production.[3,14] Therefore, to qualitatively assess the relative size of the next largest production terms, the $-\tau_{xy}\partial u/\partial x$ term was examined. Defining this term as P_2, the ratio of P_2/P can be estimated as

$$\frac{P_2}{P} \approx -\frac{1}{2}\frac{\Delta u}{u_e}\frac{\delta}{\Delta x}$$

Thus, taking the velocity difference as relative to the flat plate results ($x = 71.5$ cm), then $P_2/P \approx -0.1$ and 0.3% for the favorable and combined pressure gradient flows, respectively. Hence, compared to the additional production terms, the pressure work terms have been shown also to be very important for streamline curvature driven pressure gradient boundary layers.

Conclusions

In the present study, laser Doppler velocimetry and cross-film anemometry were used to measure the x–y Favre-averaged turbulent shear stresses and mean Favre transverse velocity fluctuation across a supersonic turbulent boundary layer, where wall curvature was used to generate a mild favorable ($\beta = -0.5$) and a combined ($\beta = 1.0$ and -1.2) pressure gradient. For comparative purposes, measurements across a zero pressure gradient equilibrium boundary layer at the same axial station were also acquired. When compared with the zero pressure gradient results, the combined streamline curvature and pressure gradient affects were found to significantly alter the turbulent shear stress. For the favorable pressure gradient flow, the magnitude across the layer was found to decrease by 50–100%. In addition, the turbulent shear stresses along the upper half of the boundary layer were found to be essentially zero. The combined pressure gradient data, though qualitatively similar, were only magnified by roughly 20%. The mean transverse Favre-averaged velocity fluctuation component was found to dramatically increase for both the favorable and combined pressure gradient flows, 170 and 300%, respectively. Finally, the present measurements suggested that the pressure work terms in the equation governing the transport of the turbulent shear stress, which arise because of compressibility and the nonzero pressure gradients, were about one order of magnitude smaller than the leading production contribution (i.e., $P_w/P \approx$ 5.0–16.0%). The remaining production terms, to which the dramatic increases in the turbulence levels have often been attributed, are generally of the same order as the pressure work. However for the present flows, these terms were estimated to be roughly an order of magnitude smaller than the pressure work terms. Thus, compressible turbulence transport models should include both for consistency.

Acknowledgment

The authors gratefully acknowledge James McMichael of the U.S. Air Force Office of Scientific Research for sponsoring this research.

References

[1]Liou, W., and Shih, T., "On the Basic Equations for Second-Order Modeling of Compressible Turbulence," NASA TM 105277, Oct. 1991.

[2]Morkovin, M., "Effects of Compressibility on Turbulent Flows," AGARD, Vol. 4, 1961, pp. 368–380.

[3]Spina, E., Smits, A., and Robinson, S., "The Physics of Supersonic Turbulent Boundary Layers," *Annual Review of Fluid Mechanics*, Vol. 26, 1994, pp. 287–319.

[4]Bradshaw, P., "Compressible Turbulent Shear Layers," *Annual Review of Fluid Mechanics*, Vol. 9, 1977, pp. 33–54.

[5]Sarkar, S., Erlebacher, G., Hussaini, M., and Kreiss, H., "The Analysis and Modeling of Dilitational Terms in Compressible Turbulence," *Journal of Fluid Mechanics*, Vol. 227, June 1991, pp. 473–493.

[6]Zeman, O., "Dilatation Dissipation: The Concept and Application in Modeling Compressible Turbulence," *Physics of Fluids*, A 2, Vol. 2, Feb. 1990, pp. 178–188.

[7]Wilcox, D., "Dilatation-Dissipation Corrections of Advanced Turbulence Models," *AIAA Journal*, Vol. 30, No. 11, 1992, pp. 2639–2646.

[8]Bowersox, R., and Schetz, J., "Model of Compressible Turbulence in Hypersonic Wall Boundary and High-Speed Mixing Layers," *AIAA Journal*, Vol. 32, No. 7, 1994, pp. 1531–1533.

[9]Smits, A., Spina, E., Alving, A., Smith, R., Fernando, E., and Donovan, J., "A Comparison of the Turbulent Structure of Subsonic and Supersonic Boundary Layers," *Physics of Fluids*, A 1, Vol. 11, Nov. 1989, pp. 1865–1875.

[10]Wilcox, D., *Turbulence Modeling for CFD*, DCW Industries, La Cañada, CA, 1993.

[11]Jayaram, M., Donovan, J., Dussauge, J., and Smits, A., "Analysis of Rapidly Distorted, Supersonic, Turbulent Boundary Layer," *Physics of Fluids*, A 1, Vol. 11, 1989, pp. 1855–1864.

[12]Dussauge, J. P., and Gaviglio, J., "The Rapid Expansion of a Supersonic Turbulent Flow: Role of Bulk Dilatation," *Journal of Fluid Mechanics*, Vol. 174, Jan. 1987, pp. 81–112.

[13]Miller, R., Dotter, J., Bowersox, R., and Buter, T., "Compressible Turbulence Measurements in Supersonic Boundary Layers with Favorable and Adverse Pressure Gradients," *2nd Symposium on Transitional and Turbulent Compressible Flows*, Joint ASME/JSME Fluids Engineering Conf., FED-Vol. 224, American Society of Mechanical Engineers, New York, 1995, pp. 193–200.

[14]Bradshaw, P., "The Effect of Mean Compression or Dilatation on the Turbulence Structure of Supersonic Boundary Layers," *Journal of Fluid Mechanics*, Vol. 63, Pt. 3, 1974, pp. 449–464.

[15]Spina, E., Donovan, J., and Smits, A., "On the Structure of High-Reynolds-Number Supersonic Turbulent Boundary Layer," *Journal of Fluid Mechanics*, Vol. 222, Jan. 1991, pp. 293–327.

[16]Waltrup, P., and Schetz, J., "Supersonic Turbulent Boundary Layer Subjected to Adverse Pressure Gradient," *AIAA Journal*, Vol. 11, No. 1, 1973, pp. 50–57.

[17]Robinson, S. K., Seegmiller, H. L., and Kussoy, M. I., "Hot-Wire and Laser Doppler Anemometer Measurements in a Supersonic Boundary Layer," AIAA Paper 83-1723, July 1983.

[18]Elena, M., and LeCharme, J., "Experimental Study of a Supersonic Turbulent Boundary Layer Using a Laser Doppler Anemometer," *Journal of Theoretical and Applied Mechanics*, Vol. 7, No. 2, 1988, pp. 175–190.

[19]Klebanoff, P. S., "Characterstics of Turbulence in a Boundary Layer with Zero Pressure Gradient," NACA Rept. 1247, 1955.

[20]Clauser, F. H., "Turbulent Boundary Layers in Adverse Pressure Gradients," *Journal of the Aeronautical Sciences*, Vol. 21, Feb. 1954, pp. 91–108.

[21]Kistler, A., "Fluctuation Measurements in a Supersonic Turbulent Boundary Layer," *Physics of Fluids*, Vol. 2, No. 3, 1959, pp. 290–296.

[22]Bowersox, R., "Thermal Anemometry," *Handbook of Fluid Dynamics and Fluids Machinery*, edited by J. Schetz and W. Fuhs, Wiley, New York, 1996, pp. 965–983.

[23]Kovasznay, L., "The Hot-Wire Anemometer in Supersonic Flow," *Journal of the Aeronautical Sciences*, Vol. 17, Sept. 1950, pp. 565–584.

[24]Spangenburg, W., "Heat-Loss Characteristics of Hot-Wire Anemometers at Various Densities in Transonic and Supersonic Flow," NACA TN 3381, May 1955.

[25]Bowersox, R., and Schetz, J., "Compressible Turbulence Measurements in a High-Speed High Reynolds Number Mixing Layer," *AIAA Journal*, Vol. 32, No. 4, 1994, pp. 758–764.

[26]Smits, A., Hayakawa, K., and Muck, K., "Constant Temperature Hot-Wire Anemometry Practice in Supersonic Flow, Part 1: The Normal-Wire," *Experiments in Fluids*, Vol. 1, No. 2, 1983, pp. 83–92.

[27]Hopkins, E., and Inouye, M., "An Evaluation of Theories for Predicting Turbulent Skin Friction and Heat Transfer on Flat Plates at Supersonic and Hypersonics Mach Number," *AIAA Journal*, Vol. 9, No. 6, 1971, pp. 993–1003.

[28]Morkovin, M., "Effects of High Acceleration on a Turbulent Supersonic Shear Layer," *Proceedings of the 1955 Heat Transfer and Fluid Mechanics Inst.*, Vol. 4, 1955, pp. 1–17.

[29]Schetz, J., *Boundary Layer Analysis*, Prentice–Hall, Englewood Cliffs, NJ, 1993.